THE JOURNAL OF NAVIGATION, Page 1 of 17.
doi:10.1017/S0373463317000893

Absolute Navigation and Positioning of Mars Rover Using Gravity-Aided Odometry

Jiandong Liu[1,2], Erhu Wei[3,4], Shuanggen Jin[1,5] and Jingnan Liu[6]

[1](*Key Laboratory of Planetary Sciences, Shanghai Astronomical Observatory, Chinese Academy of Sciences, Shanghai 200030, China*)
[2](*University of Chinese Academy of Sciences, Beijing 100049, China*)
[3](*School of Geodesy and Geomatics, Wuhan University, Wuhan 430079, China*)
[4](*Collaborative Innovation Center for Geospatial Technology, Wuhan 430079, China*)
[5](*Department of Geomatics Engineering, Bulent Ecevit University, Zonguldak 67100, Turkey*)
[6](*GNSS Research Center, Wuhan University, Wuhan 430079, China*)
(E-mail: ehwei@sgg.whu.edu.cn)

Positioning and Navigation (PN) of Martian rovers still faces challenges due to limited observations. In this paper, the PN feasibilities of Mars rovers based on a Gravity-aided Odometry (GO) system are proposed and investigated in terms of numeric simulations and a case study. Statistical features of the Mars gravity field are studied to evaluate the feature diversity of the background map. The Iterative Closest Point (ICP) algorithm is introduced to match gravity measurements with the gravitational map. The trajectories of Mars Exploration Rovers (MER) and Mars Gravity Map 2011 (MGM2011) are used to complete the experiments. Several key factors of GO including odometry errors, measurement uncertainties, and grid resolution of the map are investigated to evaluate their influences on the positioning ability of the system. Simulated experiments indicate that the GO method could provide an alternative positioning solution for Martian surface rovers.

KEYWORDS

1. Martian rover positioning. 2. Planetary rover navigation. 3. Iterative closest point. 4. Gravity-aided odometry.

Submitted: 14 April 2016. Accepted: 25 October 2017.

1. INTRODUCTION. Mars exploration has received much attention over the last few years (Jin and Zhang, 2014). The Positioning and Navigation (PN) issues for explorers or rovers have been a research focus since the 1960s (Jin et al., 2013; Wei et al., 2013; Liu et al., 2017). Among these PN designs, the Mars Exploration Rovers (MER), *Spirit* and *Opportunity*, use several integrated PN methods that are considered state-of-the-art. The

absolute positions of several initial points of the MER rovers are determined by Radio Tracking (RT) technology (Arvidson et al., 2004). The determination requires continuous tracking and would take several days, and the result is verified by the photographic feature recognition method. The differences between the two methods are within 350 m (Squyres et al., 2004). Once the first several absolute locations are determined, the rest of the trajectory is deduced by relative navigation methods which include Celestial Navigation (CN), Wheel Code Odometry (WCO), and Vision Odometry (VO) (Li et al., 2004; Arvidson et al., 2005; Squyres et al., 2006; Maimone et al., 2007). WCO is adopted for location estimation; the distance is counted by how many times the wheels have turned (wheel odometry). Then, the absolute heading (with respect to the true north of Mars) is measured by CN which uses a celestial sensor to track the line-of-sight of the Sun. VO is implemented to control the systematic errors (Li et al., 2004; Cheng et al., 2006). These methods can complete the relative positioning process, the accuracy of which is within 1 m (Maimone et al., 2007). The absolute locations of the whole trajectory are solved by integrating the RT initial points and the relative traverse.

Matthies (1989) developed Visual Odometry to estimate the motion of mobile robots by using stereo images. The key idea of the method is to detect the position and attitude changes of the rover between consecutive image pairs. The trajectory of the photographing centres can be fixed by calculating the rotation and transition relationship of the pairs. For a Mars rover, the bias between ground truth (trajectory in images) and VO are within 1 m in three axes (local system) (Li et al., 2005; Cheng et al., 2006; Maimone et al., 2007). The relative trajectory with high accuracy provides good initial information for absolute PN systems such as Gravity Odometry (GO).

The relative accuracy of VO is far better than the method proposed in this manuscript. However, the absolute position difference of the initial point between the RT results and landmarks is about 350 metres. The VO or WCO methods cannot eliminate this bias. The tracking of homonymy points of the image pairs means the VO needs large amounts of computation (Matthies et al., 2007), which causes a problem in position updating in high-speed cases. The separational determinations of absolute position and relative trajectory, provided by RT, CN, WCO and VO, cannot meet the requirements of future missions. The methods described above are time-consuming and are highly reliant on ground-based manipulation. The RT is expensive and complex to handle, even though it is currently a mature method.

Gravity Odometry (GO) could provide an alternative navigation solution, which includes near real-time absolute positioning and, to some extent, it can be operated autonomously. Jircitano and Dosch (1991) proposed the Gravity-Aided Inertial Navigation System (GAINS) for Underwater Vehicle Autonomous Navigation (UVAN). The system has been tested and several algorithms have been developed to make GAINS work for UVAN (Leonard and Bahr, 2008; Wang et al., 2016a; 2016b; Han et al., 2017). The gravity map, the accuracy of the gravity measurements (Tenzer et al., 2015a; 2015b), the matching method, and the Inertial Navigation System (INS) are key elements of the method (Wang et al., 2012; 2016a). One of the main requirements for applying the system is the large feature variations of the map along the trajectory (Zheng et al., 2013). The method could be suitable in the terrestrial planets where the gravity field is stable, which means the gravity measurements could achieve high precision. If the rover travels in a steady state the disturbance factors are extremely limited. Therefore, the transfer error of the gravity measurements to a reference such as an areoid can be controlled to a limited magnitude.

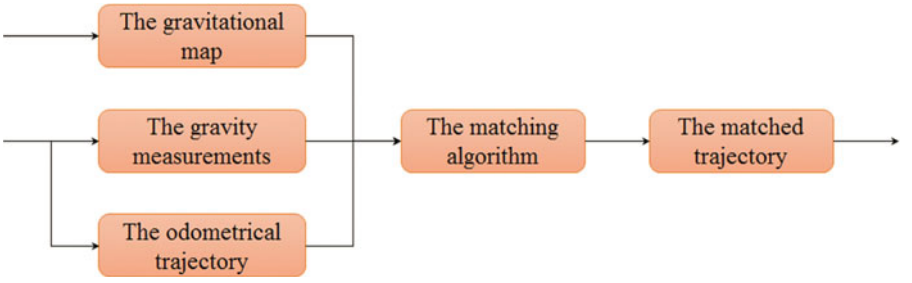

Figure 1. The flowchart of the proposed GO system. The initial trajectory is solved by integrated CN and WCO systems, which is the main PN method for Mars rovers in practical situations. The measurements used in this paper are gravity anomalies.

Second, the order and degree of improvement of the models by comprehensive measurements improves the spatial resolution of the gravity map, which provides better matching conditions. In recent decades, the GAINS system has been simulated, tested and used for UVAN. The research includes algorithm design, measurement acquirement, analysis of the map features, etc (Leonard and Bahr, 2008; Wang et al., 2016a; 2016b; Wei et al., 2017; Han et al., 2017). The functions of the INS are replaced by dead-reckoned odometry and CN heading determination in the case of planetary rover navigation as described above.

In this paper, Gravity-aided Odometry (GO) is simulated to provide PN solutions for Martian rovers. The system, which uses the relative trajectory as an input deduced by the above odometry methods, is designed to find the absolute positioning of the rovers by matching the gravity measurements with the background map. The result is the absolute position of the traverse points. We focus on investigating the PN accuracy of GO for Martian rovers under complex situations. The dead-reckoned odometry is assumed to be solved by an integrated CN and WCO method. The symmetric errors are limited by the VO. We use these trajectories deduced by CN, WCO and VO to simulate the GO. The gravity-aided dead-reckoned odometry system is presented in Section 2 as well as the structure of the autonomous navigation system. In Section 3, numerical experiments are conducted. The test results are presented to demonstrate the feasibility of the navigation system. The key factors in implementing the method are discussed in terms of initial biases, map grid resolution and accuracy of gravity measurements. Finally, the summary is given in Section 4.

2. GRAVITY-AIDED ODOMETRY NAVIGATION.

2.1. *The structure of the GO system.* Figure 1 illustrates the basic structure of a GO system (for Mars rovers), consisting of a matching algorithm with three inputs and one output. First, the dead-reckoned odometry is implemented by CN and WCO to generate the initial trajectory. Second, the gravity measurement (gravity anomaly (adopted by this paper), gravity gradient or deviation of plumb line) of each point is measured by gravimeter or gradiometer. Third, the matching algorithm (Iterative Closest Point (ICP) in this paper) is applied to search the gravity map around the initial trajectory for the optimal gravity sequence. Finally, the position corresponding to the optimal gravity sequence is regarded as the matched trajectory.

2.2. *Gravity map of Mars.* As depicted in Figure 1, the gravitational map itself has influence on the GO system, which has been extensively investigated (Wang et al., 2012; 2016b; Han et al., 2017). The attempts to investigate Mars' gravity field started at the end of the 1960s (Ash et al., 1967; Anderson et al., 1970). In most cases, the gravitational coefficients are retrieved indirectly from precise spacecraft orbits. The current harmonic coefficients of the models of the Mars gravity field can be achieved to 110 degrees and orders, for example, MRO110B (Konopliv et al., 2011). However, more sophisticated models are needed, while the MRO110B with a spatial resolution of 125 km cannot be used for navigational purposes. Hirt et al. (2012) present a model resolving the resolution down to km-scale, called the Mars Gravity Model 2011 (MGM2011). This model, which combines MRO110B2 with the Mars Orbiter Laser Altimeter (MOLA) topographic model to estimate the short-scale waves (scales of ∼3 km to ∼125 km), provides surface gravity accelerations and vertical deflections over the entire Martian surface at 3 arcmin resolution. The grid resolution of the map is higher than 2·964 km × 2·964 km (semimajor axis a = 3,395,428 m).

The statistical properties of the gravity map have a significant influence on the GO system since the core idea of the algorithm is serial correlation (Wang et al., 2016a). Several statistical indices, such as variance, global absolute value of roughness, or slope variance, can be used to evaluate the feature diversity of the gravity map. The indices were used to estimate the topographic features. The absolute value of the roughness of an arbitrary point, however, is the most straightforward and useful property to describe the variations of the gravity feature.

Assuming $g(i,j)$ is the gravity anomaly at a given point (i,j), the roughness R_G of the point is the arithmetic mean value of the roughness in two orthogonal directions R_B and R_L:

$$R_G = (R_B + R_L)/2 \tag{1}$$

The subscripts B and L represents the latitude and longitude direction (dimensionless), respectively. The roughness of the two directions is estimated by computing the expected value of the absolute difference of the adjacent points:

$$\begin{aligned} R_L &= E\,|g(i,j) - g(i,j+1)| \\ R_B &= E\,|g(i,j) - g(i+1,j)| \end{aligned} \tag{2}$$

Figure 2(a) and Figure 3(a) show the $3' \times 3'$ (MGM2011) roughness of gravity map of *Opportunity* and *Spirit*, respectively. Figure 2(b) and Figure 3(b) are the $0{\cdot}25' \times 0{\cdot}25'$ (by interpolation) cases. The map roughness around *Opportunity* is larger than *Spirit* in most of the image except for some peak values at the edge of the map. Moreover, the traverse points of the rovers are in the middle of the image. The gravity field around the trajectory of *Opportunity* is rougher.

2.3. *The Matching algorithm.* The matching algorithm used in this paper is called Iterative Closest Point (ICP). Besl and McKay (1992) proposed the algorithm which is based on point-to-point quaternion matching and has been improved many times (Champleboux et al., 1992; Chen and Medioni, 1991; Zhang, 1994). A high-quality overview of the ICP can be seen in Pomerleau et al., 2015). The idea of the ICP is to find the closest values to the measurements in a background database, which calculates the correlation function of the observations and the matched values iteratively. The relationship between

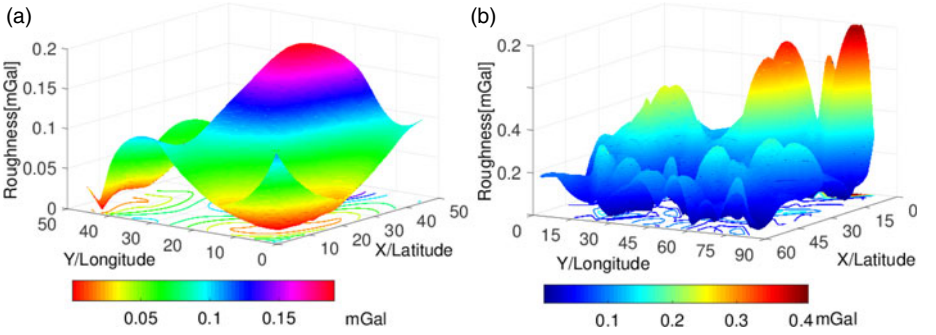

Figure 2. The roughness of gravity map of *Opportunity*. (a) grid interval $3' \times 3'$, (b) $0{\cdot}25' \times 0{\cdot}25'$. The curve on the underside are roughness isolines of the anomaly. The colour bar represents the roughness value of the map. The X, Y represents latitude and longitude direction (dimensionless), respectively. (a) and (b) are the same area. They have different matrix dimensions.

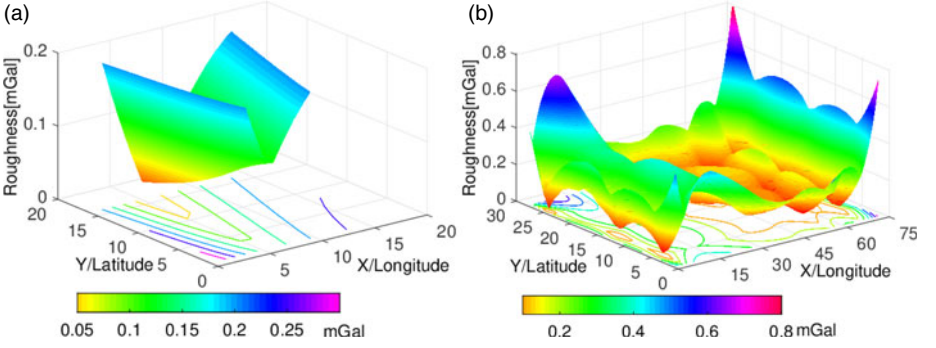

Figure 3. The roughness of gravity map of *Spirit*. (a) the grid interval is $3' \times 3'$, (b) $0{\cdot}25' \times 0{\cdot}25'$.

the closest values $\vec{p}'_{ri}$ and the observations $\vec{p}_{ri}$ can be transferred by rotation $R(\vec{q}_R)$ and translation $\vec{q}_T$ as:

$$\vec{p}'_{ri} = R(\vec{q}_R)\vec{p}_{ri} - \vec{q}_T \tag{3}$$

The elements of the rotation matrix $R(\vec{q}_R)$ are the maximum eigenvector of the correlation function matrix aligned by quaternion (Pomerleau et al., 2015). In that way, the difference between $\vec{p}_{ri}$ and $\vec{p}'_{ri}$ is

$$\Delta f = \left|\vec{p}'_{ri} - \vec{p}_{ri}\right| \tag{4}$$

The computational process will end if $\Delta f < \tau$ or the iterations are greater than the iterated thresholds. τ is a threshold value.

We use an ICP point-to-point algorithm in this paper for simulation convenience. The method is also adopted partly because the matching process can be completed within several tens of seconds and because the accuracy analysis would be clear and straightforward by using this method. The method can also keep a matched trajectory such as the simulated one.

2.4. *The odometrical trajectories.* The trajectory data of the twin rovers of MER, *Opportunity* and *Spirit,* have been used in this paper (Li et al., 2005; Matthies et al., 2007).

The number of coordinate points for *Spirit* is 393 and for *Opportunity* is 1068. The grid resolution (by interpolation) of the maps used in the experiments is $0{\cdot}25' \times 0{\cdot}25'$ described above for experiments in Sections 3.1 and 3.2. The whole relative trajectories of the rovers are set as one of the inputs. The number of interations is 30 for Sections 3.1 and 3.2 and it is 1000 for Section 3.3. The increase of the iterations is to keep the matched results more stable. The true trajectory is acquired from comprehensive positioning results determined by CN, WCO, and VO (Li et al., 2004; 2005; Matthies et al., 2007). The odometrical results of the MER rovers by the above methods are accurate, which can be used as an initial input to the GO system. Therefore, the biases added in Section 3 are assumed to be constant or errors with systematic growth.

3. NUMERICAL EXPERIMENTS AND RESULTS.

3.1. *The experiments with different magnitude initial errors.*

3.1.1. *The experimental condition.* The initial errors of the MER rovers are about 350 m. These errors will influence the ICP matching process. GO experiments with different magnitude initial errors are introduced in this section. The simulated trajectory is generated by adding biases into the true trajectory:

$$\begin{aligned} B_{sim} &= B_{real} + \delta B \\ L_{sim} &= L_{real} + \delta L \end{aligned} \tag{5}$$

where the subscript "sim" represents the simulated traverse and "real" is the true trajectory. δB and δL are the latitudinal and the longitudinal position biases, respectively. There are six different magnitude errors, which are $\delta B = \delta L = [0{\cdot}01^\circ\ 0{\cdot}008^\circ\ 0{\cdot}006^\circ\ 0{\cdot}004^\circ\ 0{\cdot}003^\circ\ 0{\cdot}002^\circ]$. The distance (on Mars' surface) approximates D = [592 m 492 m 392 m 292 m 192 m 92 m]. The threshold value τ to end the ICP process is set as $\tau = 2 \times 0{\cdot}25'$. The accuracy of the gravity anomaly can be up to 0·01 mGal (Lederer, 2009; Creutzfeldt et al., 2014). Considering the differences between the map and measurements, 0·1 mGal random errors are added to the simulated measurements:

$$g_m = g_{real} + rand(\pm 0{\cdot}1) \tag{6}$$

In Equation (7), g_m are the gravity anomaly measurements. g_{real} is the true value. The "rand" means random function.

3.1.2. *Experimental results.*

3.1.2.1. *Experimental result of Mars Spirit.* Two results are illustrated in Figure 4. The matching results for *Spirit* are illustrated in Figures 4(a) and 4(b) in which the initial errors are 600 m and 300 m, respectively. It is shown that the matching trace (green) drifts completely from both the true traverse (red) point and simulated traverse (blue) in Figure 4(a). The matching trace (green) is close to the true trajectory (red) in Figure 4(b). This indicates the GO system has successfully decreased the initial error.

The errors between the true trace and the matched trajectory are portrayed in Figures 5(a) and 5(b). The errors illustrated in the two figures show that the GO system has failed when the initial biases are greater than 500 m. The matching process is partially successful when the initial bias is about 400 m. The reason why some parts of the matching trace drift from the true trace is discussed in Section 3.4. The initial bias is significantly decreased when the magnitude of the bias is lower than 300 m. The longitude errors are within 110 m and the latitude errors are within 60 m.

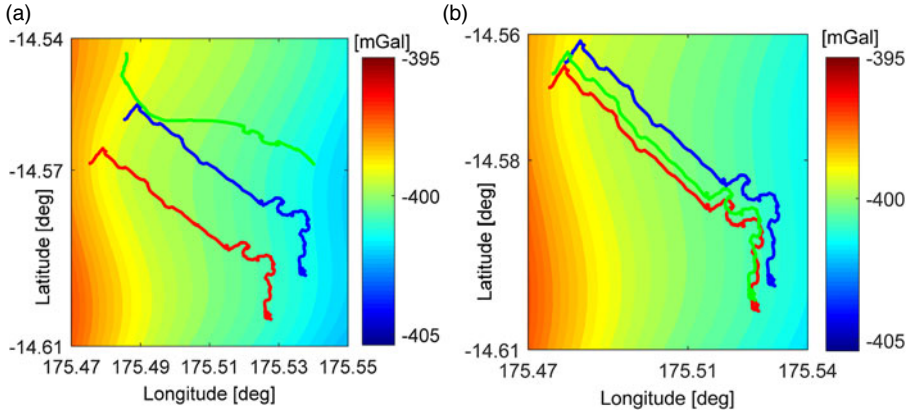

Figure 4. Two matching results between matched trajectory (green) and true trajectory (red) of *Spirit* when initial bias is about (a) 600 m and (b) 300 m, respectively. The blue trajectory in (a) and (b) means traverse deduced by dead-reckoned odometry. The colour bars represent gravity anomaly value. The meaning of the symbols and colours used here is same as in Figure 6.

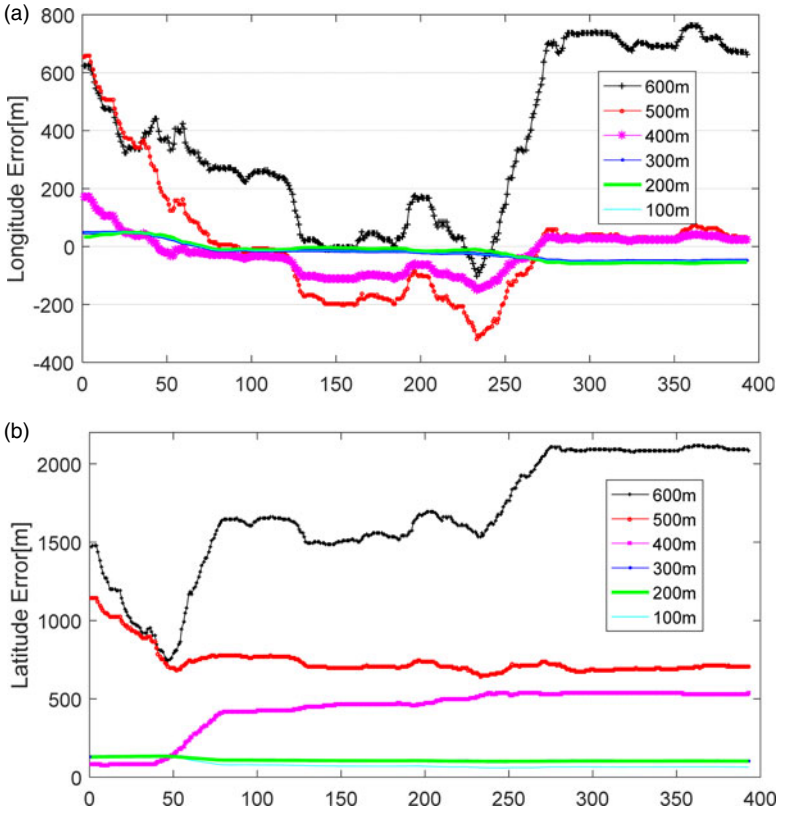

Figure 5. (a) Longitude Error and (b) Latitude Error of the matching traverse in different initial bias (100–600 m) compared with the true trajectory of the *Spirit* Rover.

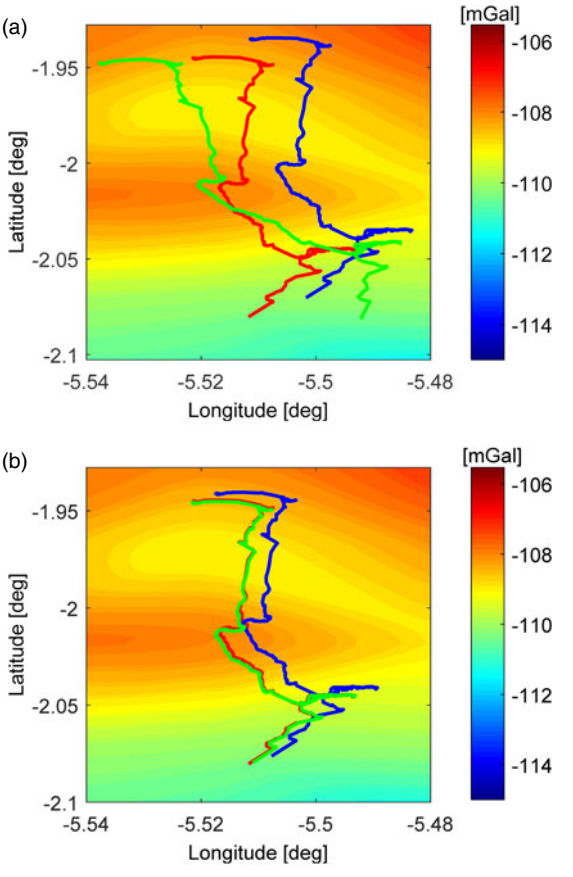

Figure 6. Two matching results for *Opportunity* when initial bias is about (a) 600 m and (b) 300 m, respectively.

3.1.2.2. *Experimental results of Mars Opportunity*. The true trajectory (red), simulated trajectory (blue), and matched trajectory (green) are illustrated in Figure 6. The initial bias is approximately 600 m in Figure 6(a) and 300 m in Figure 6(b).

As is portrayed in Figures 7(a) and 7(b), the difference between matched position and true trajectory is within 1100 m in longitude and is within 200 m in latitude. When the initial error goes down to around 0·008°, the point before the 1000th point is close to the true position. The difference is reduced by 300 m in longitude when the initial bias is 0·006°. The GO achieves perfect matching when the initial bias equals 0·004°. The difference in both directions remains within 60 metres. When the initial error is reduced to a lower magnitude, the improvement of the positioning result is limited.

The absolute positioning results of the initial point (with simulated initial error 400 m) are compared with RT techniques and photographic feature comparison. The results are presented in Table 1. The results acquired by our method are in accordance with the current method. The differences between our method and photographic comparison are small. These results show the method has potential to be an alternative to current absolute-positioning techniques such as RT. The positioning errors of GO can be as large as 1000 m

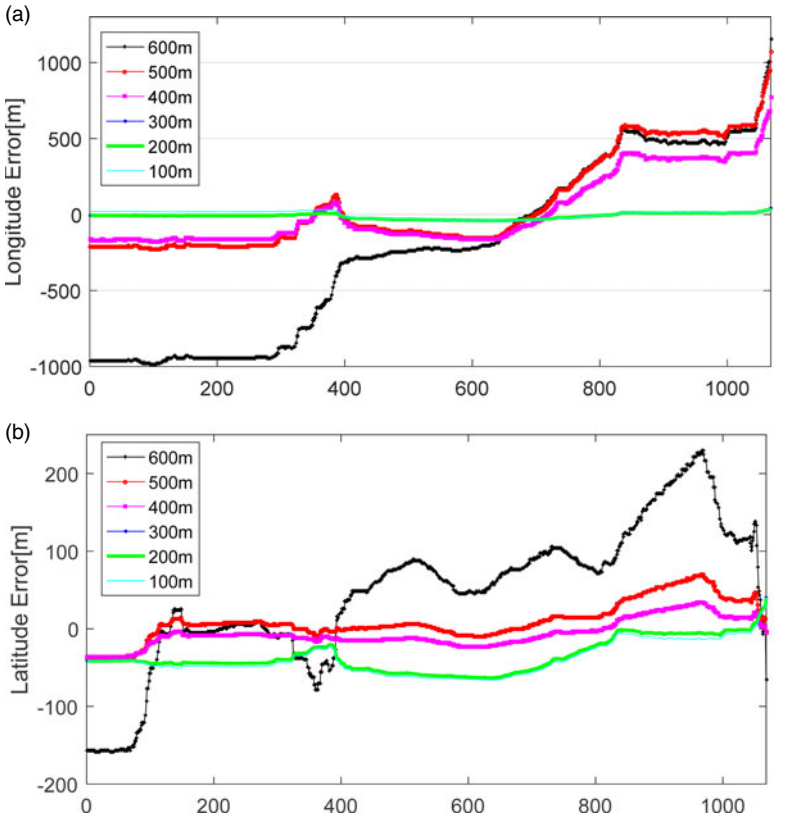

Figure 7. (a) Longitude Error and (b) Latitude Error of the matching traverse in different initial bias compared with the true trajectory of the *Opportunity* Rover.

Table 1. Absolute positioning results compared with other techniques.

Positioning techniques and bias	MER-A(*Spirit*)		MER-B(*Opportunity*)	
Radio tracking	175·47848°E	14·571892°S	354·47417°E	1·9483°S
Photograph feature comparison	175·4729°E	14·5692°S	354·4734°E	1·9462°S
Position bias/degree	0·00558°	0·002692°	0·00077°	0·0021°
Position bias/metre	330·678662m	159·531672m	45·6312588m	124·448955m
Positioning results of this paper	175·4774399E	14·56667786S	354·473670131°E	1·944713097°S
Bias compared with RT/degree	0·001040113°	0·005214136°	0·000499869°	0·003586903°
Bias compared with RT/metre	61·604048426m	308·823927723m	29·60635326m	212·4457993m
Compared feature comparison/ degree	−0·004539887°	0·002522136°	−0·000270131°	0·001486903°
Compared feature comparison/ metre	−268·889322081m	149·381606324m	−15·99936274m	88·06657381m

at some points as shown in Figure 7, but the system could be an in-situ, real-time, and autonomous navigational scheme.

3.2. *Experiments with systematic cumulative error of the odometry.* The calculated tracks of the rovers will have a large bias from the true trajectory because of the cumulative

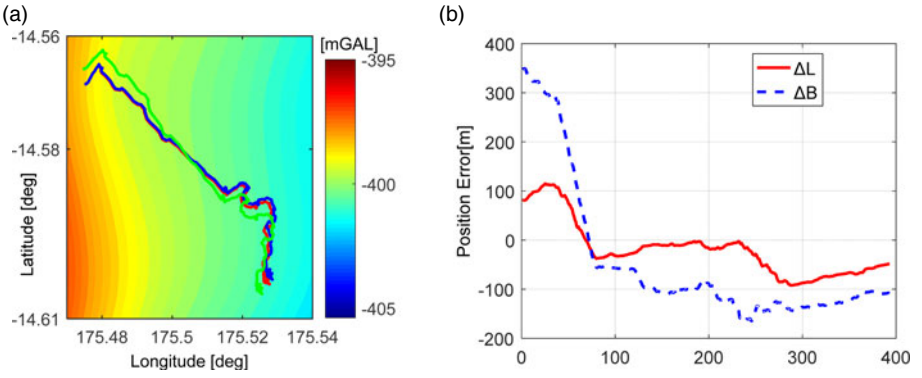

Figure 8. Matching differences between matched trajectory and real (true) trajectory of *Spirit* with increasing cumulative error (maximum about 110 metres). (a) matching result, and (b) the position errors between the true trajectory and matched trajectory.

error caused by the odometry system. In fact, the rovers' calculated track will deviate from its normal path. The WCO and VO techniques cannot eliminate the systematic errors.

3.2.1. *The experimental condition.* We assume the initial errors have been reduced to within acceptable limits by the GO system described in Section 3.1. That is, the position bias of several points at the beginning between the simulated trajectory and the true trajectory is small. The simulated track is generated as follows:

$$\begin{aligned} B_{sim} &= B_{real} + N \times 0{\cdot}017/3600 \\ L_{sim} &= L_{real} + N \times 0{\cdot}017/3600 \end{aligned} \tag{7}$$

In Equation (7), the meaning of the subscripts of longitude L and latitude B are the same as in Equation (5). N is the number of points. For *Spirit*, N = 393 and *Opportunity* N = 1068. The grid interval of the gravity maps of Mars are $0{\cdot}25' \times 0{\cdot}25'$. The measurements of gravity anomaly are generated from Equation (6).

3.2.2. *Experimental results.* The matched trajectory of *Spirit* converges to the true track after the 75th point, in which the position biases are within 170 m in two directions. The results are illustrated in Figures 8(a) and 8(b). The matched trajectory (green) portrayed in Figure 8(a) indicates that the matching process is not perfect. The reason is the gravity field around the track is so smooth that the gravity feature cannot be extracted by the ICP algorithm. As portrayed in Figure 9, the matched trajectory of *Opportunity* converges to the true track quickly, and the position errors are also within 170 m in two directions.

3.3. *Experiments with other parameters.* The relationships between positioning results and the map uncertainty as well as the grid resolution of the map are discussed in this section. The initial errors added to the simulation trajectory equals 400 m.

3.3.1. *The uncertainty of the gravity map.* The uncertainty of the gravity map to the positioning results is discussed in term of different magnitude bias (0·1 mGal, 0·5 mGal and 1 mGal) between the map and the real gravity value. The grid resolution is $0{\cdot}25' \times 0{\cdot}25'$. The positioning errors are shown in Figure 10. The blue line is latitude error and the black line represents longitude error. The ICP algorithm can tolerate a map uncertainty of 1 mGal in the region where the gravity field is coarser, such as in the area around *Opportunity*. The tolerance is 0·5 mGal in the region around *Spirit*. Statistical results are shown in Table 2. In

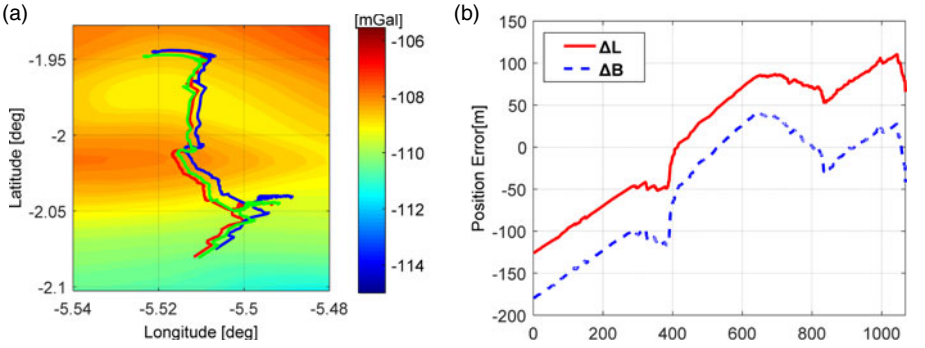

Figure 9. Matching differences between matched trajectory and real (true) trajectory of *Opportunity* with increasing cumulative error (maximum about 300 metres). (a) matching result, and (b) the position errors between the true trajectory and matched trajectory.

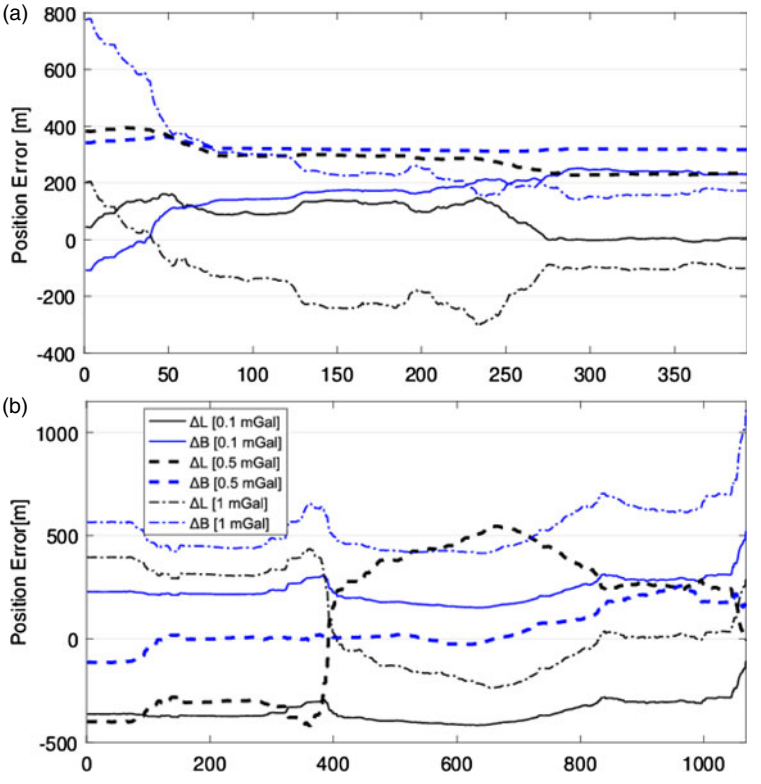

Figure 10. The positioning error with respect to different uncertainty of the gravity map. (a) *Spirit* (b) *Opportunity*.

most cases, the positioning errors are within 500 m for both *Spirit* and *Opportunity*, which suggests the GO could achieve considerable accuracy in practical situations. The mismatch of some points can be adjusted by other suitable algorithms. The ICP or other algorithms should be improved to tolerate larger map uncertainties up to 2–3 mGal. For an underwater

Table 2. Statistical results with different gravity uncertainties.

	ΔL	0·1 mGal		ΔB	ΔL	0·5 mGal		ΔB	ΔL	1 mGal		ΔB
	max mean	min SD	max mean	min SD	max mean	min SD	max mean	min SD	max mean	min SD	max mean	min SD
MER-A	161·3 76·9	−8·08 56·1	251·0 164·9	−108·7 83·8	394·5 285·5	227·3 49·7	362·7 323·5	311·2 13·2	204·5 −129·3	−303·0 99·4	778·1 269·8	142·0 149·0
MER-B	−495·7 −101·8	−182·2 201·0	504·8 250·1	227·2 93·7	565·5 59·1	−398·4 261·1	245·7 58·2	−103·8 130·78	435·4 78·2	−236·0 220·85	1107·7 530·3	415·13 107·3

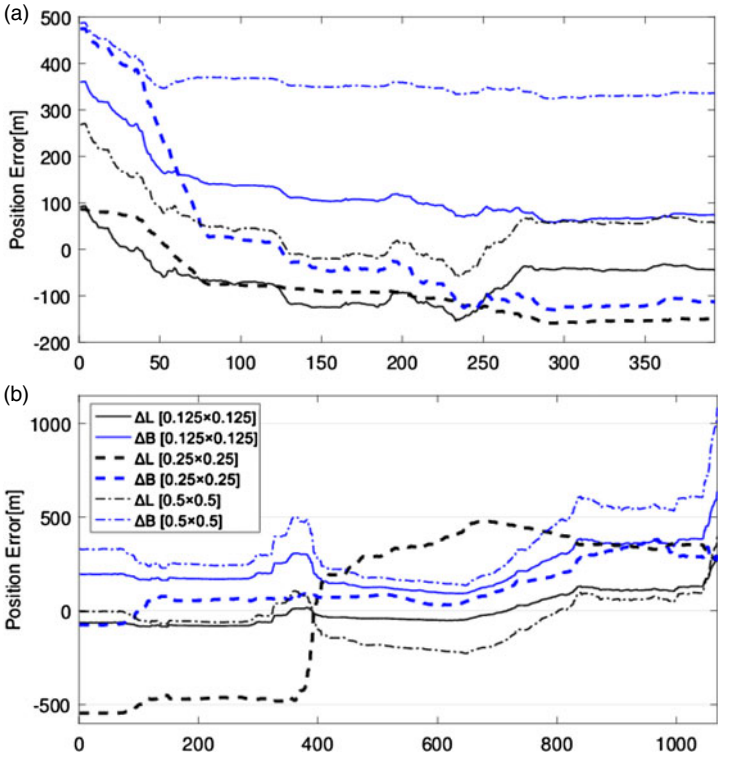

Figure 11. The positioning results with different map spatial resolution. (a) *Spirit* (b) *Opportunity*.

case, the level is about 3-5 mGal (Wei et al., 2017). The uncertainties are smaller if the measurements are observed in stable circumstances.

3.3.2. *The grid interval of the gravity map.* The relationship between the grid resolution and the positioning results is analysed in this section. The errors are illustrated in Figure 11. The grid intervals of the map are $0{\cdot}125' \times 0{\cdot}125'$, $0{\cdot}25' \times 0{\cdot}25'$, and $0{\cdot}5' \times 0{\cdot}5'$. The initial errors added to the simulation trajectory equal 400 m. The measurement uncertainty is 0·1 mGal. The blue line shows errors in latitude and the black one represents the longitude differences. A gravity map with a higher grid interval is needed. A low-resolution map could introduce large positioning errors as shown in Figure 11. The statistical results

Table 3. Statistical results with different background resolution.

	ΔL	0·125′ × 0·125′		ΔB	ΔL	0·25′ × 0·25′		ΔB	ΔL	0·5′ × 0·5′		ΔB
	max	min	max	min	max	min	max	min	max	min	max	min
	mean	SD	mean	SD	mean	SD	mean	SD	mean	SD	mean	SD
MER-A	84·7	−159·5	356·1	37·0	269·8	−59·9	487·0	323·8	86·0	−159·1	474·2	−130·3
	−82·6	48·1	105·3	77·5	47·7	64·5	355·9	32·6	−89·0	70·1	1·7	168·1
MER-B	299·8	−83·1	637·7	92·7	478·1	−546·0	381·6	−75·5	402·3	−226·7	1084·0	136·4
	0·8	80·0	222·9	102·5	46·9	407·8	121·4	120·8	−48·4	110·8	343·2	166·9

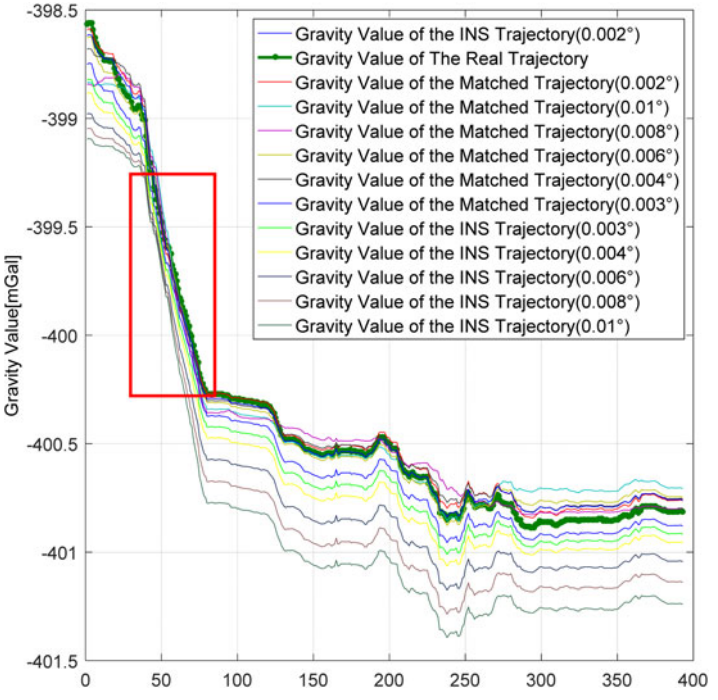

Figure 12. The profile line of gravity anomaly of the *Spirit* trajectory with different magnitude initial error.

are shown in Table 3. The improvements of the grid resolution are dependent on the increase of the order and degree of the models. This also needs both satellite and ground-based (on the surface of Mars) measurements. Most of the positioning accuracies are within 500 m.

The results listed in Table 3 indicate a high grid resolution gravity map is needed because most of the positioning errors correlate with the grid intervals. The grid interval D should be set as small as possible. Table 3 shows that the grid interval of the map is important for the method, in which the lower resolution will mislead the matching process and result in position uncertainties.

3.4. *Feasibility analysis.* For the two cases, the Gravity-aided Odometry (GO) system can achieve a considerably improved positioning result compared with traditional

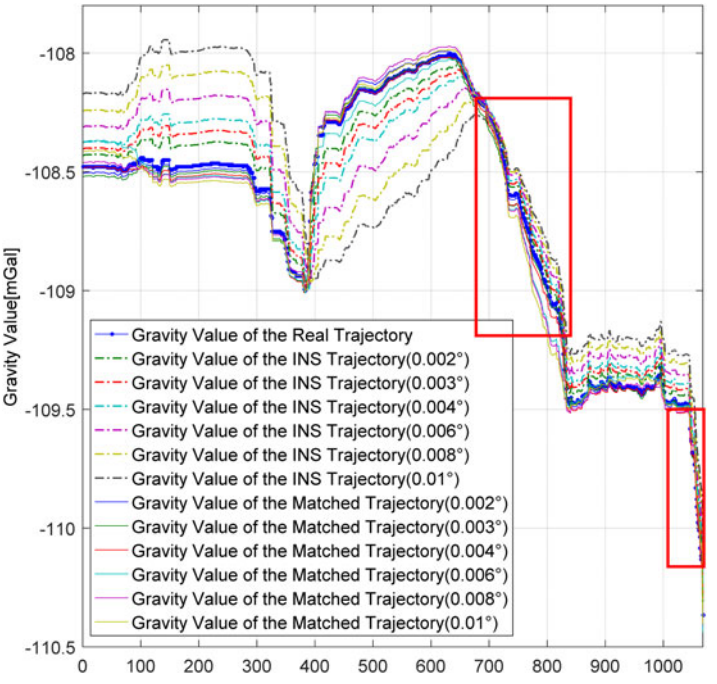

Figure 13. The profile line of gravity anomaly of the *Opportunity* trajectory with different magnitude initial error.

methods. The system tolerates initial errors with a magnitude up to 500 m where the diversity of the gravity field is larger. The tolerance is about 300 m in a smoother gravity field. The ICP algorithm tolerates map uncertainty up to 1 mGal in the coarser gravity field around the *Opportunity* regions. A higher accuracy gravity map with lower uncertainty is important to the GO system for rover positioning and autonomous navigation. The GO requires a higher stage-order gravity field to improve both map accuracy and spatial resolution. Moreover, the grid resolution of the map should be as high as possible.

Incorrect matching occurs in the region where the gravity profile lines of the trajectory overlap each other (lines within red rectangle blocks in Figures 12 and 13). This is due to the features of the ICP algorithm. If the profile lines of the different tracks overlap each other in some regions, the matching result will mislead the algorithm, slipping into the wrong position.

The GO system is highly feasible even though the position bias was large in some cases. The resolution of the map can be improved by new measurements from a Martian orbiter. The uncertainty of the measurements can be limited by using a high accuracy gravity meter or gradiometer and related algorithm. Real-time navigation can be solved by integrating a Kalman Filter with the matching method, as implemented in underwater applications (Wang et al., 2016b; Wei et al., 2017). The gradient of the gravity could provide more abundant observation information which could improve the positioning accuracy.

4. SUMMARY AND DISCUSSION. The experiments have unequivocally validated the feasibility of a gravity-aided odometry system, which uses a gravity anomaly map to conduct absolute positioning of a rover on Mars' surface. The experiments demonstrate the property of the gravity map, the uncertainties between measurements and the map values, and that the algorithm itself has a pivotal influence on the positioning results.

The results are better in higher diversity regions. The GO system with an ICP matching algorithm can tolerate initial uncertainties as large as 400 m in areas lacking diversity. The tolerance approximates 800 m in feature-rich regions. The initial locations provided by RT can fulfil the requirements. The positioning ability of GO approximates 200–600 m in the *Spirit* and *Opportunity* MER regions. The uncertainties of gravity anomalies should be limited to some extent such as 1 mGal when ICP is used to conduct the matching. The ICP operates stably if the grid interval equals 0·5′. The ICP is suitable in the case study but might be impractical in real-time navigation due to the iteration and algorithm characteristics. The worst positioning accuracies under our assumptions are within 500 m. The initial trajectory required by the GO can be easily fulfilled by RT and VO. The absolute locations of the rovers provided by current RT or GO described in the paper can meet the reference demands that Mars Global Mapping requires. The relative accuracy can be satisfied by VO during surface exploration.

It is important to note there will be some challenges in practical use. The potential problems are:

(1) A gravity map of Mars with higher spatial resolution and accuracy is necessary, and the stage-order of the models should be improved by future observations.
(2) An algorithm for real-time navigation needs to be developed and tested in practice, which is solved by combined Kalman filter with Terrain Contour Matching (TERCOM) in the case of UVAN (Wang et al., 2016b; Wei et al., 2017).
(3) A high accuracy gravimeter or gradiometer will be needed on board the rover, since current Martian gravity observations are from indirect retrieval methods.

ACKNOWLEDGEMENTS

This research is supported by the National Natural Science Foundation of China (Grant No. 41374012). The authors would like to thank the anonymous reviewers who reviewed and helped improve this manuscript.

REFERENCES

Anderson, J.D., Efron, L. and Wong, S.K. (1970). Martian mass and Earth-Moon mass ratio from coherent S-band tracking of Mariners 6 and 7. *Science*, **167**(3916), 277–279.

Arvidson, R.E., Anderson, R.C., Bartlett, P., Bell, J.F., Blaney, D., Christensen, P.R. and Ferguson, R. (2004). Localization and physical properties experiments conducted by Spirit at Gusev Crater. *Science*, **305**(5685), 821–824.

Arvidson, R.E., Squyres, S.W., Anderson, R.C., Bell III, J.F., Blaney, D., Brueckner, J. and Clark, B.C. (2005). Overview of the Spirit Mars Exploration Rover Mission to Gusev Crater: Landing Site to Backstay Rock in the Columbia Hills. *Journal of Geophysical Research: Planets (1991–2012)*, **111**(E2), 1–22.

Ash, M.E., Shapiro, I.I. and Smith, W.B. (1967). Astronomical constants and planetary ephemerides deduced from radar and optical observations. *The Astronomical Journal*, **72**(3), 338–350.

Besl, P.J. and McKay, N.D. (1992). A method for registration of 3-D shapes. *Pattern Analysis and Machine Intelligence*, *IEEE Transactions on*, **14**(2), 239–256.

Champleboux, G., Lavallee, S., Szeliski, R. and Brunie, L. (1992). From accurate range imaging sensor calibration to accurate model-based 3D object localization. *Computer Vision and Pattern Recognition, IEEE*, 83–89.

Chen, Y. and Medioni, G. (1991). Object modelling by registration of multiple range images. *Robotics and Automation*, *IEEE*, 2724–2729.

Cheng, Y., Maimone, M.W. and Matthies, L. (2006). Visual odometry on the Mars exploration rovers-a tool to ensure accurate driving and science imaging. *Robotics & Automation Magazine*, **13**(2), 54–62.

Creutzfeldt, B., Troch, P.A., Guntner, A., Ferre, T., Graeff, T. and Merz, B. (2014). Storage discharge relationships at different catchment scales based on local high precision gravimetry. *Hydrological Processes*, **28**(3), 1465–1475.

Han, Y., Wang, B., Deng, Z., Wang, S., and Fu, M. (2017). A mismatch diagnostic method for TERCOM-based underwater gravity aided navigation. *IEEE Sensors Journal*, **17**(9), 2880–2888.

Hirt, C., Claessens, S.J., Kuhn, M. and Featherstone, W.E. (2012). Kilometer-resolution gravity field of Mars: MGM2011. *Planetary and Space Science*, **67**(1), 147–154.

Jin, S.G. and Zhang, T.Y. (2014). Automatic detection of impact craters on Mars using a modified adaboosting method. *Planetary and Space Science*, **99**, 112–117.

Jin, S., Arivazhagan, S., and Araki, H. (2013). New results and questions of lunar exploration from SELENE, Chang'E-1, Chandrayaan-1 and LRO/LCROSS. *Advances in Space Research*, **52**(2), 285–305.

Jircitano, A. and Dosch, D.E. (1991) Gravity aided inertial navigation system (GAINS). *Institute of Navigation, 47th Annual Meeting*, **1**, 221–229.

Konopliv, A.S., Asmar, S.W., Folkner, W.M., Karatekin, Ö., Nunes, D.C., Smrekar, S.E., and Zuber, M.T. (2011). Mars high resolution gravity fields from MRO, Mars seasonal gravity, and other dynamical parameters. *Icarus*, **211**(1), 401–428.

Lederer, M. (2009). Accuracy of the relative gravity measurement. *Acta Geodyn Geomater*, **6**(3), 383–390.

Leonard, J.J. and Bahr, A. (2008). Autonomous underwater vehicle navigation. *IEEE Journal of Oceanic Engineering*, **35**(3), 663–678.

Li, R., Di, K., Matthies, L.H., Folkner, W.M., Arvidson, R.E. and Archinal, B.A. (2004). Rover localization and landing-site mapping technology for the 2003 Mars exploration rover mission. *Photogrammetric Engineering & Remote Sensing*, **70**(1), 77–90.

Li, R., Squyres, S.W., Arvidson, R.E., Archinal, B.A., Bell, J., Cheng, Y. and Golombek, M. (2005). Initial results of rover localization and topographic mapping for the 2003 Mars Exploration Rover mission. *Photogrammetric Engineering & Remote Sensing*, **71**(10), 1129–1142.

Liu, J., Wei, E., and Jin, S. (2017). Mars Cruise Orbit Determination from Combined Optical Celestial Techniques and X-ray Pulsars. *The Journal of Navigation*, **70**(4), 719–734.

Maimone, M., Cheng, Y., Matthies, L. (2007). Two years of visual odometry on the mars exploration rovers. *Journal of Field Robotics*, **24**(3), 169–186.

Matthies, L., Maimone, M., Johnson, A., Cheng, Y., Willson, R., Villalpando, C. and Angelova, A. (2007). Computer vision on Mars. *International Journal of Computer Vision*, **75**(1), 67–92.

Matthies, L.H. (1989). Dynamic stereo vision. *Doctoral Dissertation, Carnegie Mellon University Pittsburgh*, PA, USA.

Pomerleau, F., Colas, F. and Siegwart, R. (2015). A review of point cloud registration algorithms for mobile robotics. *Foundations and Trends in Robotics (FnTROB)*, **4**(1), 1–104.

Squyres, S.W., Arvidson, R.E., Bell, J.F., Bruckner, J., Cabrol, N.A., Calvin, W. and Des Marais, D.J. (2004). The Opportunity Rover's Athena science investigation at Meridiani Planum. *Science*, **306**(5702), 1698–1703.

Squyres, S.W., Arvidson, R.E., Bollen, D., Bell, J.F., Brueckner, J., Cabrol, N.A. and Crumpler, L. (2006). Overview of the Opportunity Mars exploration rover mission to Meridiani Planum: Eagle Crater to Purgatory Ripple. *Journal of Geophysical Research: Planets*, **111**(E12).

Tenzer, R., Eshagh, M. and Jin, S.G. (2015b). Martian sub-crustal stress from gravity and topographic models. *Earth and Planetary Science Letters*, **425**, 84–92.

Tenzer, R., Chen, W., Tsoulis, D., Bagherbandi, M., Sjoberg, L., Novak, P. and Jin, S.G. (2015a), Analysis of the refined CRUST1·0 crustal model and its gravity field. *Surveys in Geophysics*, **36**(1), 139–165.

Wang, B., Yu, L., Deng, Z., and Fu, M. (2016b). A particle filter-based matching algorithm with gravity sample vector for underwater gravity aided navigation. *IEEE/ASME Transactions on Mechatronics*, **21**(3), 1399–1408.

Wang, B., Zhu, Y., Deng, Z., and Fu, M. (2016a). The gravity matching area selection criteria for underwater gravity-aided navigation application based on the comprehensive characteristic parameter. *IEEE/ASME Transactions on Mechatronics*, **21**(6), 2935–2943.

Wang, H., Wang, Y., Fang, J., Chai, H. and Zheng, H. (2012). Simulation research on a minimum root-mean-square error rotation-fitting algorithm for gravity matching navigation. *Science China Earth Sciences*, **55**(1), 90–97.

Wei, E., Dong, C., Liu, J., Yang, Y., Tang, S., Gong, G. and Deng, Z. (2017). A robust solution of integrated SITAN with TERCOM algorithm: weight-reducing iteration technique for underwater vehicles' gravity-aided inertial navigation system. *Navigation*, **64**, 111–122.

Wei, E., Jin, S.G., Zhang, Q., Liu, J., Li, X. and Yan, W. (2013). Autonomous navigation of Mars probe using X-ray pulsars: Modeling and results. *Advances in Space Research*, **51**(5), 849–857.

Zhang, Z. (1994). Iterative point matching for registration of free-form curves and surfaces. *International Journal of Computer Vision*, **13**(2), 119–152.

Zheng, H., Wang, H., Wu, L., Chai, H. and Wang, Y. (2013). Simulation research on gravity-geomagnetism combined aided underwater navigation. *The Journal of Navigation*, **66**(01), 83–98.